Chapter 25B. Analysis of Imaging Spectrometer Data for the South Helmand Area of Interest

By Todd M. Hoefen and Stuart A. Giles

Abstract

Hyperspectral data collected over the South Helmand area of interest (AOI) in southern Afghanistan were analyzed with spectroscopic methods to identify the occurrence of selected material classes at the surface. Absorption features in the spectra of HyMap data were compared to a reference library of spectra of known materials. The HyMap data in this AOI are limited by the southern edge of the dataset and the southern border of Afghanistan. Calcite + montmorillonite and illite account for almost 90 percent of the mapped pixels in the South Helmand AOI. Chlorite or epidote group minerals, muscovite, kaolinite, alunite, jarosite, and pyrophyllite occur in spatially localized patterns throughout the region. Fe^{2+} Fe^{3+} Type 2, Fe^{3+} Type 1, Fe-hydroxide, and goethite dominate the iron-bearing mineral map of the AOI. Illite, Fe^{3+} Type 1, and Fe-hydroxide are mapped in contiguous areas that are consistent with aeolian sediments detected in the TM data. Calcite + montmorillonite and Fe^{2+} Fe^{3+} Type 2 group minerals are mapped in areas that have exposed bedrock that appears to be relatively free of sand and dust. Coherent groupings of hematite and jarosite are also present. Hematite appears to be a weathering product of the rocks surrounding the intrusive bodies in the northwestern region of the AOI. There are six known prospects of aragonite within the South Helmand AOI, but this area is highlighted as a region of potential porphyry copper-gold mineralization. The presence of jarosite, alunite, kaolinite and pyrophyllite in the HyMap data further suggests that this region does contain significant porphyry copper-gold mineralization. Several of these locations are identified within the HyMap data and are discussed in this chapter and a companion anomalies report.

25B.1 Introduction

Past studies of geologic data of Afghanistan indicated areas with the potential for a variety of minerals resources (Peters and others, 2007; Abdullah and others, 1977). Several of these areas were selected for follow-on studies using imaging spectroscopy data to characterize surface materials. One such area is the South Helmand area of interest (AOI) in southern Afghanistan, which is approximately 700 kilometers (km) southwest of Kabul (fig. 25B–1). The area has the potential for aragonite, travertine/onyx, porphyry copper, porphyry copper-gold and skarn copper (gold) deposits. To help assess these potential resources, high-resolution imaging spectrometer data were analyzed to detect the presence of selected minerals that may be indicative of past mineralization processes. This report contains the results of the spectroscopic data analyses and identifies sites within the South Helmand AOI that warrant further investigation, especially detailed geological mapping, lithologic sampling, and geochemical studies.

25B.2 Data Collection and Processing

In 2007, imaging spectrometer data were acquired over most of Afghanistan as part of the U.S. Geological Survey (USGS) project "Oil and Gas Resources Assessment of the Katawaz and Helmand Basins." These data were collected to characterize surface materials in support of assessments of resources (coal, water, minerals, oil, and gas) and earthquake hazards in the country (King and others, 2010). Imaging spectrometers measure the reflectance of visible and near-infrared light from the Earth's surface in many narrow channels, producing a reflectance spectrum for each image pixel. These reflectance spectra can be interpreted to identify absorption features that arise from specific chemical transitions and molecular bonds that provide compositional information about surface materials. Imaging spectrometer data can only be used to characterize the upper surface materials and not subsurface composition or structure. Subsurface processes can be indicated, however, by the distribution of surface materials.

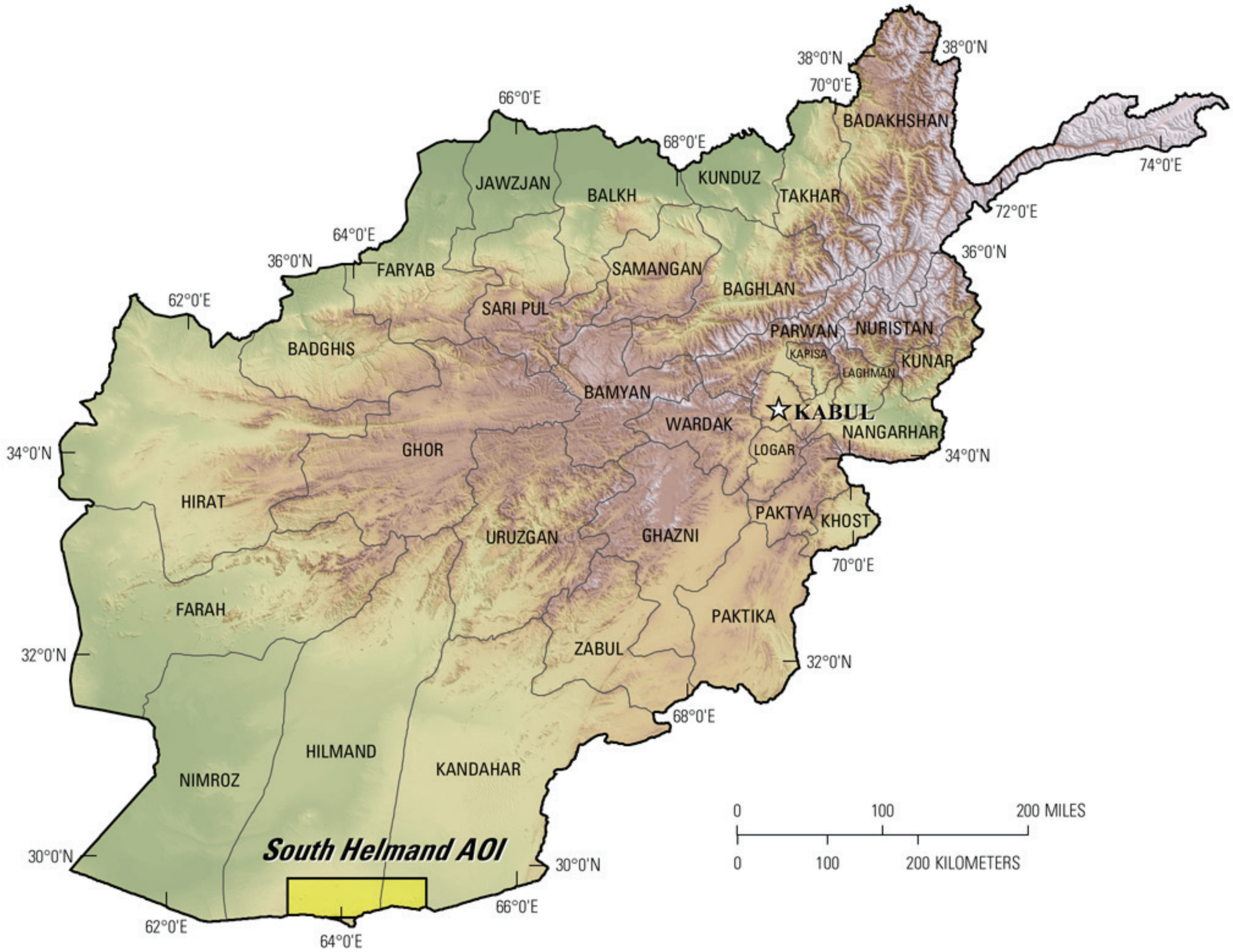

Figure 25B–1. Index map of the South Helmand area of interest, northestern Afghanistan.

25B.2.1 Collection of Imaging Spectrometer Data

The HyMap imaging spectrometer (Cocks and others, 1998) was flown over Afghanistan from August 22 to October 2, 2007 (Kokaly and others, 2008). HyMap has 512 cross-track pixels and covers the wavelength range from 0.43 to 2.48 microns (µm) in 128 channels. The imaging spectrometer was flown on a WB-57 high altitude aircraft at 50,000 feet. There were 207 standard data flight lines and 11 cross-cutting calibration lines collected over the country of Afghanistan for a total of 218 flight lines, covering a surface area of 438,012 square kilometers (km^2) (Kokaly and others, 2008). Data were received in scaled radiance (calibrated to National Institute of Standards and Technology reference materials). Before processing, four channels that had low signal-to-noise and (or) were in wavelength regions that overlapped between detectors were removed from the image cubes. Each flight line was georeferenced to Landsat base imagery in Universal Transverse Mercator (UTM) projection (Davis, 2007).

25B.2.2 Calibration Process

HyMap data were converted from radiance to reflectance using a multi-step calibration process. This process removed the influence of the solar irradiance function, atmospheric absorptions and residual instrument artifacts, resulting in reflectance spectra that have spectral features that arise from the material composition of the surface. Because of the extreme topographic relief and restricted access to ground calibration sites, modifications to the standard USGS calibration procedures were required to calibrate the 2007 Afghanistan HyMap dataset (Hoefen and others, 2010). In the first step of the calibration process, the radiance data were converted to apparent surface reflectance using the radiative transfer correction program Atmospheric CORrection Now (ACORN; ImSpec LLC, Palmdale, Calif.). The ACORN program was run multiple times for each flight line, using average elevations in 100-meter (m) increments, covering the range of minimum to maximum elevations encountered within the flight line. A single atmospherically corrected image was assembled from these elevation-incremented ACORN results, by determining the elevation of each HyMap pixel and selecting the atmospherically corrected pixel from the 100-m increment closest to that elevation.

Each assembled atmospherically corrected image was further empirically adjusted using ground based reflectance measurements from a ground calibration site. Five ground calibration spectra were collected in Afghanistan: Kandahar Air Field, Bagram Air Base, and Mazar-e-Sharif Airport, as well as, soil samples from two fallow fields in Kabul. At each site, the average field spectrum of the ground target was used to calculate an empirical correction factor using the pixels of atmospherically corrected HyMap data in the flight lines that passed over the site. Subsequently, each of the HyMap flight lines was ground-calibrated using the empirical correction from the closest calibration site.

To further improve the data quality, an additional calibration step was taken to address the atmospheric differences caused, in part, by the large distances between the calibration sites and the survey areas. The large distances were the result of a lack of safe access to ground calibration sites. The duration of the airborne survey and variation in time of day during which flight lines were acquired also resulted in differences in atmospheric conditions between standard flight lines and lines over ground calibration sites, which were used to derive the empirical correction factors. Over the course of the data collection process, the sun angle, atmospheric water vapor, and atmospheric scattering differed for each flight line. To compensate for this variation, cross-cutting calibration flight lines over the ground calibration areas were acquired (Kokaly and others, 2008) and used to refine the reflectance calculation for standard data lines. A multiplier correction for standard data lines, typically oriented as north-south flight lines, was derived using the pixels of overlap with the well-calibrated cross-cutting lines, subject to slope, vegetation cover and other restrictions on pixel selection (Hoefen and others, 2010). As a result, the localized cross-calibration multiplier, derived from the region of overlap, reduced residual atmospheric contamination in the imaging spectrometer data that may have been present after the ground calibration step.

25B.2.3 Materials Maps and Presentation

After undergoing the above calibration process, the georeferenced and calibrated reflectance data were processed. The reflectance spectrum of each pixel of HyMap data was compared to the spectral features of reference entries in a spectral library of minerals, vegetation, water, and other materials (King, Johnson, and others, 2011; Kokaly and others, 2011). The best spectral matches were determined for each pixel and the results were clustered into classes of materials discussed below.

HyMap reflectance data were processed using MICA (Material Identification and Characterization Algorithm), a module of the U.S. Geological Survey Processing Routines in Interactive Data Language (IDL) for Spectroscopic Measurements (PRISM) software (Kokaly, 2011). The MICA analysis compared the reflectance spectrum of each pixel of HyMap data to entries in a reference spectral library of minerals, vegetation, water, and other materials. The HyMap data were compared to

97 reference spectra of well-characterized mineral and material standards. The resulting maps of material distribution, resampled to 23 × 23-m square pixel grid, were mosaicked to create thematic maps of surface mineral occurrences over the full data set covering Afghanistan.

The MICA module was applied to HyMap data twice to present the distribution of two categories of minerals naturally separated in the wavelength regions of their primary absorption features. MICA was applied using the subset of minerals with absorption features in (1) the visible and near-infrared wavelength region, producing the 1-µm map of iron-bearing minerals and other materials (King, Kokaly, and others, 2011), and (2) the shortwave infrared region to produce the 2-µm map of carbonates, phyllosilicates, sulfates, altered minerals, and other materials. For clarity of presentation, some individual classes in these two maps were bundled by combining selected mineral types (for example, all montmorillonites or all kaolinites) and representing them with the same color in order to reduce the number of mineral classes. The iron-bearing minerals map portrays 28 classes. Iron-bearing minerals with different mineral compositions but similar broad spectral features are difficult to classify as specific mineral species. Thus, generic spectral classes, including several minerals with similar absorption features, such as Fe^{3+} Type 1 and Fe^{3+} Type 2 are depicted on the map. The carbonates, phyllosilicates, sulfates, and altered minerals map has 32 classes. Minerals with slightly different compositions but similar spectral features are less easily distinguished, therefore, some identified classes consist of several minerals with similar spectra, such as the “chlorite or epidote” class. When comparisons with reference spectra provided no viable match, a designation of “not classified” was assigned to a pixel.

25B.3 Geologic Setting of the South Helmand Area of Interest

The South Helmand AOI is within the Helmand (also spelled “Hilmand”) and Kandahar Provinces in southern Afghanistan and covers approximately 6,628 km^2. The contrast-enhanced stretch of the natural color composite of Landsat Thematic Mapper (TM) bands in figure 25B–2 provides a general overview of the South Helmand AOI terrain and is useful for understanding the general characteristics and distribution of surficial material, including rocks and soil, unconsolidated sediments, vegetation, and hydrologic features. The TM image shows areas of aeolian deposition in shades of yellow-brown and the bedrock in shades of gray. The Chaigai Hills lie along the southern border of the AOI as darker units.

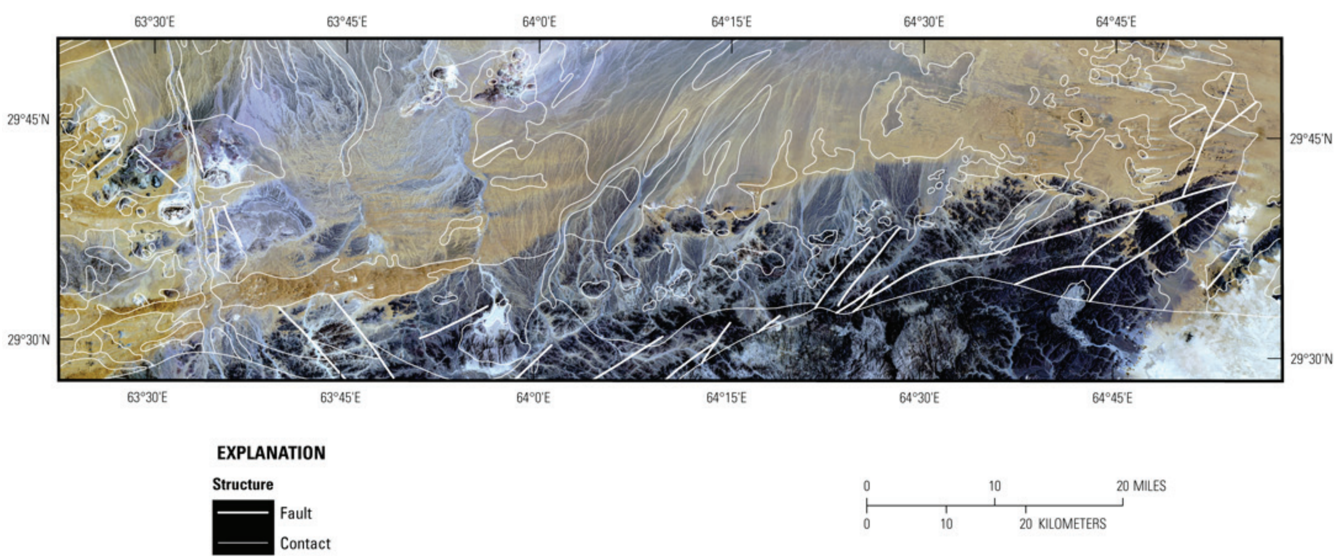

Figure 25B–2. Contrast Enhanced Landsat Thematic Mapper natural color image of the South Helmand area of interest. Geologic units and faults from (Doebrich and Wahl, 2006; Abdullah and Chmyriov, 1977).

25B.3.1 Topography

Elevations in the South Helmand AOI range from 835 to 2,174 m (fig. 25B–3). The lowest areas within the South Helmand AOI are in the Helmand Basin in the northern and eastern regions of the AOI. The highest areas are within the south-central and southwestern regions of the AOI in the Chaigai Hills.

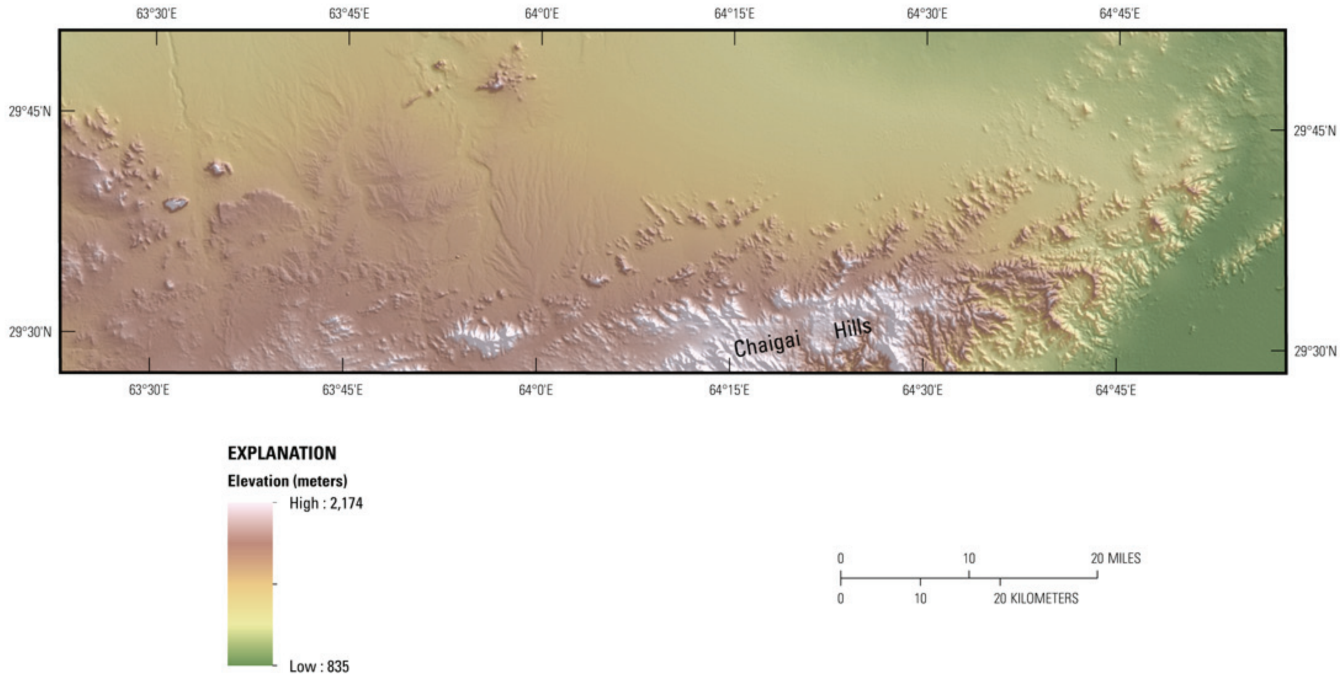

Figure 25B–3. Elevations and topography of the South Helmand area of interest.

25B.3.2 Lithology and Structure

Two fault zones are present in the AOI; the first is a southeast-northwest trending fault system in the western region of the AOI, and the other is a southwest-northeast trending fault system that extends from the south-central region and parallels the Afghanistan-Pakistan border (figs. 25B–1 and 25B–4). Faulting is mostly in Cretaceous age rocks at high elevations.

Rocks in the South Helmand area range in age from Oligocene to Recent. Quaternary stratified formations compose most of the units in the northern and western region of the AOI. A large unit of Early Pliocene rocks occurs just east of the western fault zone. Cretaceous (undifferentiated) stratified formations occur at high elevations near the Pakistan and Afghanistan border and extend into the northeastern and northwestern parts of the AOI. Intrusive rocks of Oligocene and Early Quaternary age also occur within the AOI. Early Quaternary age intrusive rocks are present in the western region whereas Oligocene intrusive rocks are dispersed throughout the eastern part of the AOI (fig. 25B–4; Doebrich and Wahl 2006; Abdullah and Chmyriov, 1977). The Oligocene age intrusive rocks consist of granite, granite porphyry, granodiorite, quartz syenite, and granosyenite, whereas the Early Quaternary intrusive rocks are rhyodacite.

25B.3.3 Known Mineralization

Figure 25B–5 shows six locations where mineralization with a potential for mineral resource development may exist (Peters and others, 2007; Doebrich and Wahl 2006; Abdullah and Chmyriov, 1977). Only aragonite (travertine) prospects are present as known prospects within the South Helmand AOI. The mineralogical characteristics of the mineral prospects are summarized in table 25B–1.

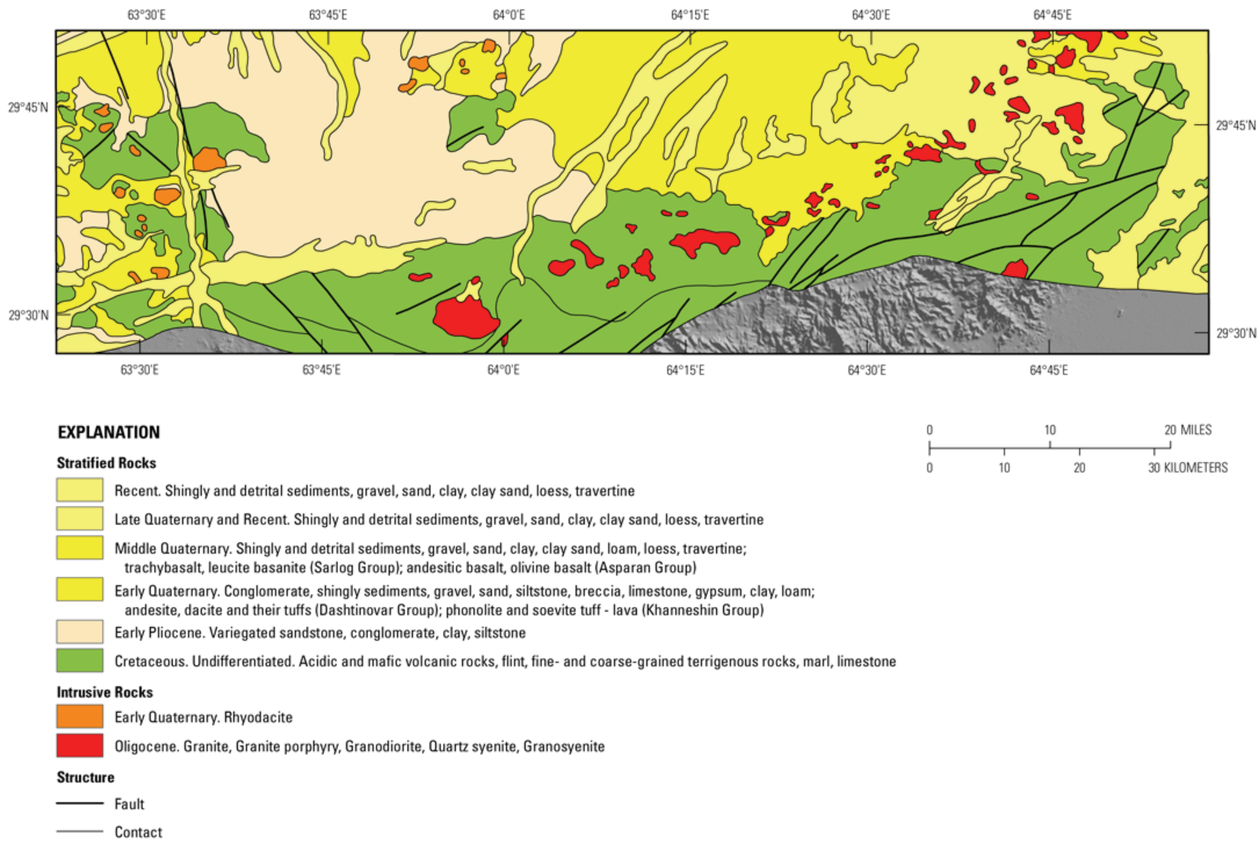

Figure 25B–4. Geologic map of the South Helmand area of interest from 1:500,000-scale geologic map of Afghanistan (Doebrich and Wahl 2006; Abdullah and Chmyriov, 1977).

The Sukhlog, Malik Dukan, Panawuk and Muzdan prospects all occur within Eocene to Oligocene volcanic rocks as sheet-like lodes or veins. Thicknesses range from 0.5 to 20 m and can extent up to 500 m. The Zoldag prospect occurs at the contact of Early Quaternary subvolcanic bodies and Pliocene units in bedded veins that are 50 m thick and can extend for 250 m. The host lithology for the Argu prospect is Early Quaternary andesite-dacite subvolcanic rocks that are 0.4 to 4.0 m thick and can extend for 100 to 250 m (Peters and others, 2007; Abdullah and others, 1977).

The Chaigai Hills are permissive for the occurrence of porphyry copper, porphyry copper-gold, and skarn copper prospects (Peters and others, 2007). Several porphyry copper deposits and prospects are present near the Afghanistan border in Pakistan (Dasht-e-Kain, Ziarat Pir Sultan, Saindak, Koh-i-Dalil, Reko Diq), but there are no known deposits within the South Helmand AOI (Peters and others, 2007). The Dasht-e-Kain porphyry copper deposit is a porphyry copper-gold deposit associated with Early Miocene (21 Ma) breccia and tonalite porphyry; the Saindak deposit is also dated at about 21 Ma. The largest deposit is Reqo Dik occurrence, which contains andesite, andesite agglomerate, diorite, granodiorite and granite (Ahmad, 1992; Ahmad and others, 1986; Breitzman and others, 1983; Kazmi and Qasim, 1997; Leaman and Staude, 2003; Sillitoe and Khan, 1977; Sillitoe, 1978; Spector and others, 1987; Perello and others, 2008). Rocks similar to those found in Pakistan occur in the Chaigai Hills of Afghanistan, increasing the potential for porphyry copper-gold mineralization in this area. The area in and around the South Helmand AOI was subdivided into three separate permissive tracts or porphyry copper and porphyry copper-gold prospects by Peters and others (2007), who estimated approximately three undiscovered prospects were likely in the area. Mars and Rowan (2007) used the advanced spaceborne thermal emission and reflection radiometer (ASTER) to map potential areas of phyllic and argillic altered rocks within this region as well.

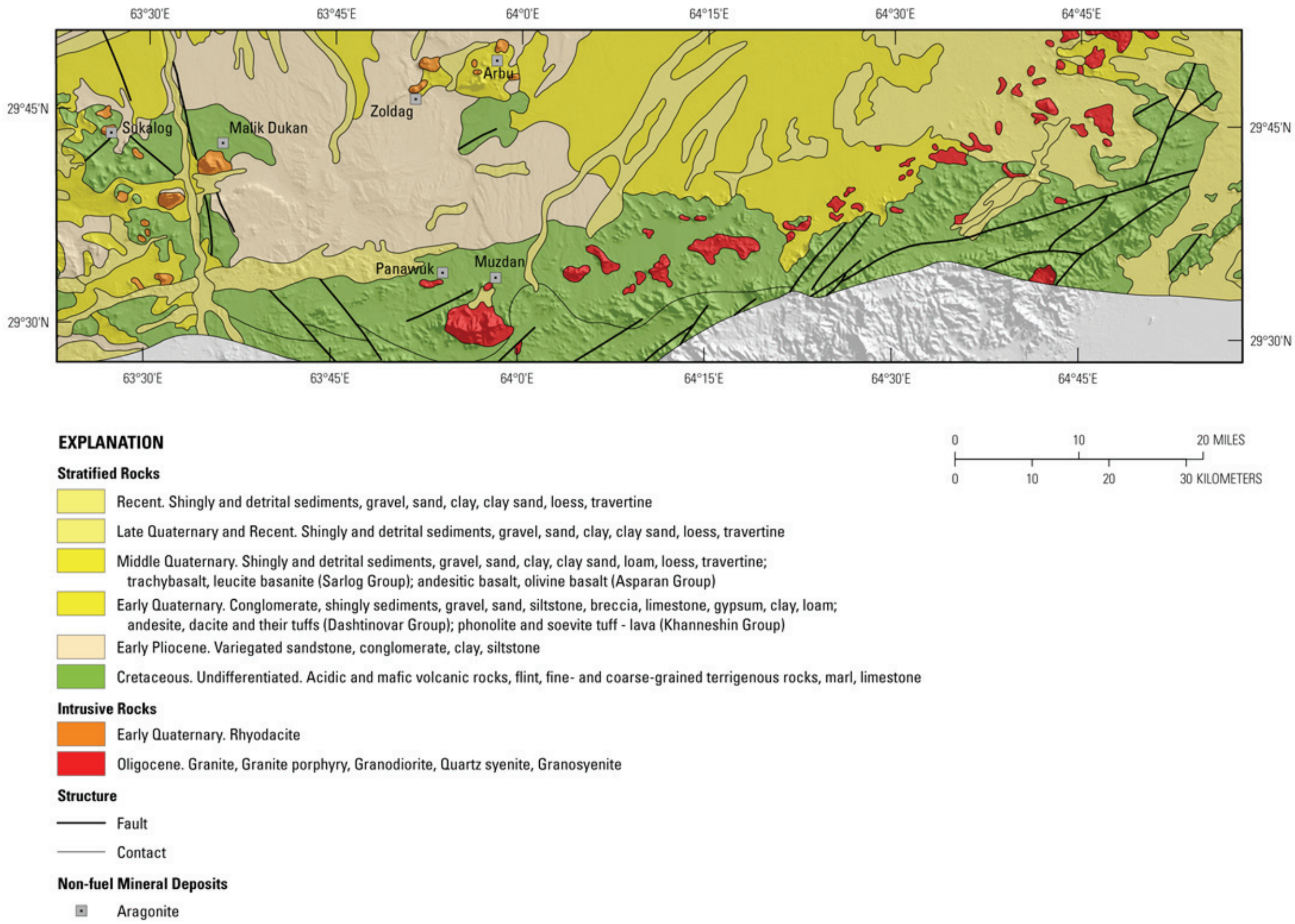

Figure 25B–5. Sites of known mineralization by deposit type (Peters and others, 2007) on the geologic map of the South Helmand area of interest from 1:500,000-scale geologic map of Afghanistan (Doebrich and Wahl 2006; Abdullah and Chmyriov,1977).

Table 25B–1. Sites of known sites of mineralization in the South Helmand area of interest (Doebrich and Wahl 2006; Abdullah and Chmyriov,1977; Peters and others, 2007).

[—, no known alteration associated with the given deposit type]

Name	Deposit type	Alteration	Mineralogy	Gangue
Muzdan	Aragonite	—	Aragonite	No data
Panawuk	Aragonite	—	Aragonite	No data
Malik Dukan	Aragonite	—	Aragonite	No data
Sukalog	Aragonite	—	Aragonite	No data
Zoldag	Aragonite	—	Aragonite	No data
Arbu	Aragonite	—	Aragonite	No data

25B.3.4 Data Limitations

Geographic registration between various data sets is not always possible because of differences in data collection methods and resolution. The geographic accuracy and quality of each data set is limited by the quality of the original source. Significant efforts were made to ensure the geographic accuracy of the HyMap data; however, exact registration between previously published known mineral occurrences, fault traces, geologic units, and structural boundaries in comparison to the HyMap data may not be ideal. To resolve additional details, the digital versions of these maps can be viewed at a higher spatial resolution than what is possible on a single page printed map.

25B.4 Mineral Maps of the South Helmand Area of Interest

Analysis of the HyMap imaging spectrometer data of the South Helmand AOI using spectroscopic methods resulted in the identification of a wide variety of minerals exposed at the surface. Although the occurrence of certain minerals may suggest that mineralization processes may have once operated in the area, many of the minerals that were identified are also common rock-forming minerals or minerals that can be derived from the weathering of a wide variety of rock types. Consequently, the distribution patterns of the identified minerals and the geologic context in which they occur are essential for understanding the causes of mapped mineral occurrences and evaluating the possible potential for related mineral deposits.

Figures 25B–6 and 25B–7 depict, respectively, the distribution of the carbonates, phyllosilicates, sulfates, altered minerals, and other materials (32 possible classes), and the iron-bearing minerals (28 possible classes) for the South Helmand AOI.

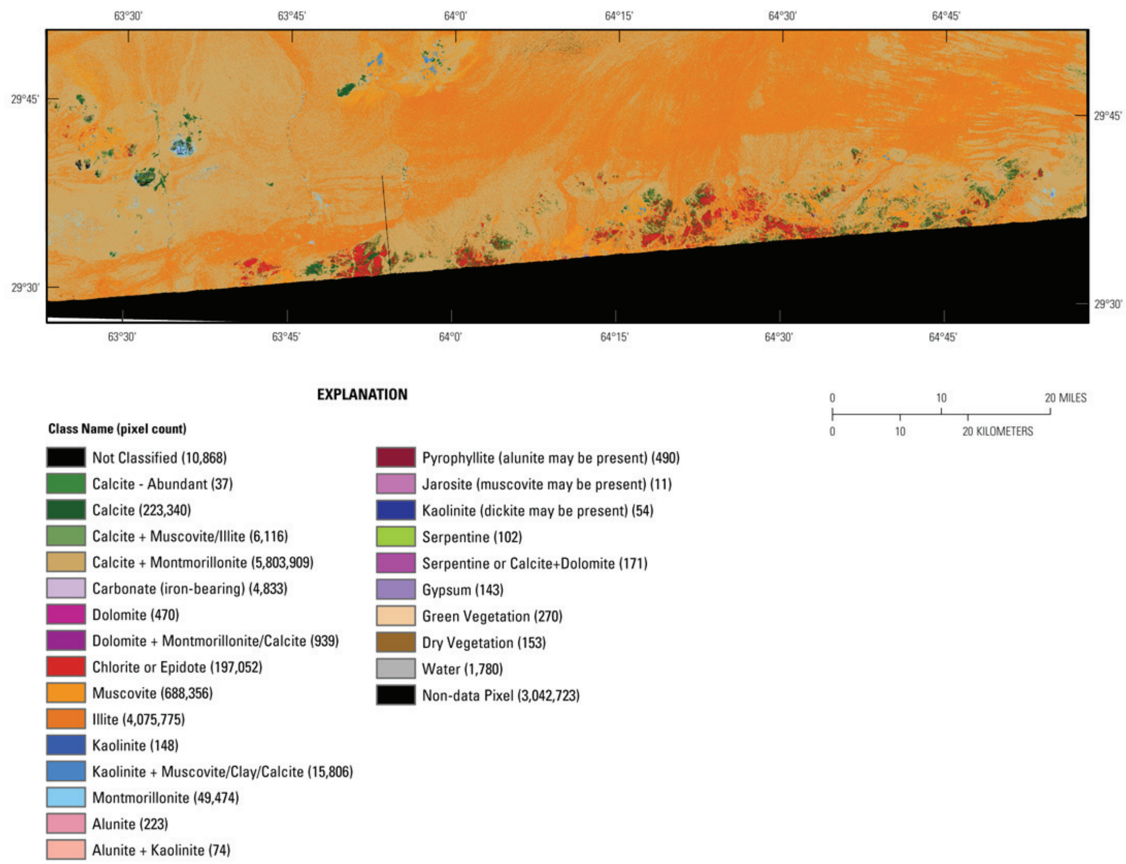

Figure 25B–6. Map of carbonates, phyllosilicates, sulfates, altered minerals, and other materials derived from HyMap data in the South Helmand area of interest.

In the iron-bearing minerals map (fig. 25B–7), the Fe^{2+} Fe^{3+} Type 2 and Fe^{3+} Type 1 classes dominate the AOI, with large, spatially coherent patterns of goethite, Fe-hydroxide, hematite, and Fe^{2+} Type 1. Most of the Fe^{3+} Type 1 and Fe-hydroxide classes coincide with aeolian features in the TM data (fig. 25B–2). The Fe-hydroxide class matches the dark brown/yellow color in the TM data and the Fe^{3+} Type 1 class matches the lighter shades of brown/yellow. Fe^{2+} Fe^{3+} Type 2 material appears to be present in the upper bedrock units where windblown dusts have scoured the surface. Iron-bearing materials were not mapped within the known intrusive bodies in many areas, suggesting that there is a lack of iron minerals within these units. Because of the large number of classes represented and the subtleties of the distribution patterns, it is instructive to display these results as a series of image maps, each depicting a selected group of minerals that are mineralogically related or commonly occur together in specific geologic environments (figs. 25B–8 through 25B–12). Figure 25B–8 shows the distribution of carbonate minerals in the South Helmand AOI, and figure 25B–9 shows the distribution of clay minerals and micas. The distribution of iron oxide and hydroxide minerals are displayed in figure 25B–10. Minerals commonly found in hydrothermally altered rocks are mapped in figure 25B–11, and secondary minerals often associated with mineralized and/or weathered rocks are mapped in figure 25B–12.

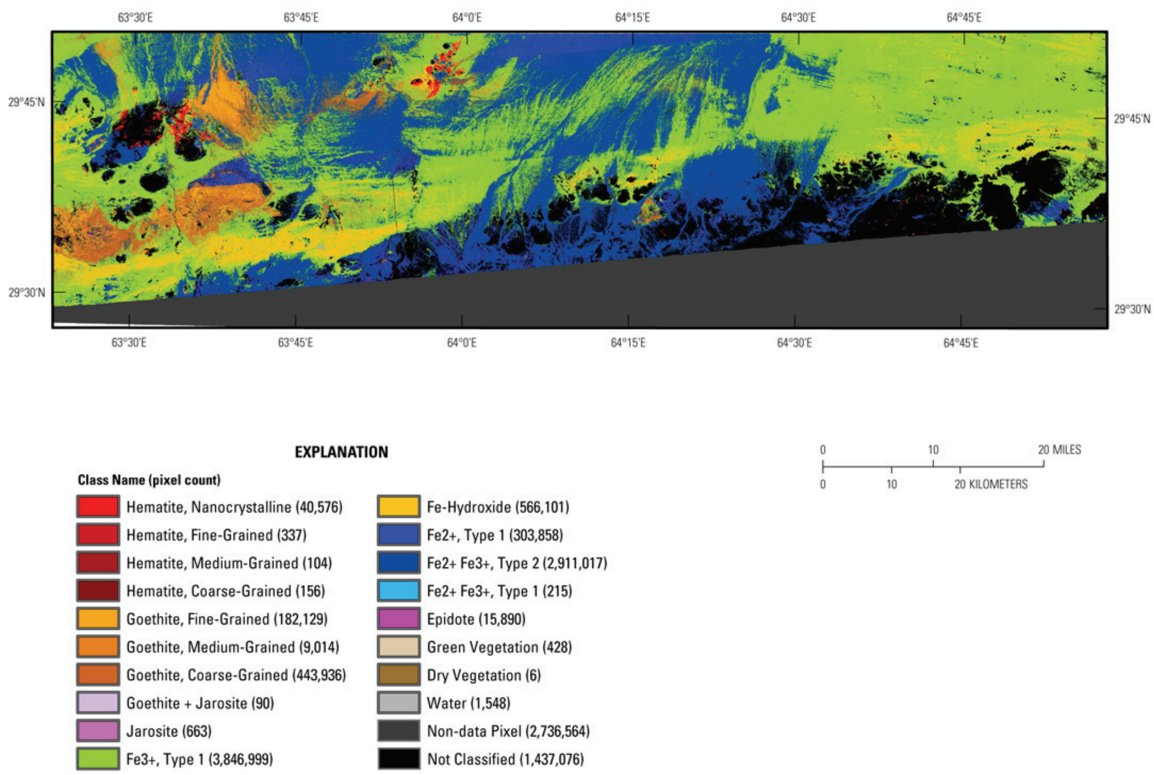

Figure 25B–7. Map of iron-bearing minerals and other materials derived from HyMap data in the South Helmand area of interest.

25B.4.1 Carbonate Minerals

In general, the carbonates are mapped throughout the AOI and within almost every geologic unit. The six known mineral occurrences are all mapped within one of the four calcite classes. Calcite + montmorillonite or illite mineral groups account for almost 90 percent of the mapped pixels in this AOI and occur in almost every rock unit (fig. 25B–8). A comparison to the TM data (figure 25B–2) suggests that the aeolian materials map mostly as the illite class whereas the upper bedrock units tend to map as calcite + montmorillonite mineral group. Contiguous areas of calcite or calcite + muscovite/illite map within Cretaceous (undifferentiated) stratified formations and are consistent with the rocks that compose this unit (Doebrich and Wahl 2006; Abdullah and Chmyriov, 1977). Calcite is also mapped in or near Early Quaternary intrusive rocks in the western (lat 29°42'12"N., long 63°35'54"E.) and northwestern regions of the AOI (lat 29°46'29"N., long 63°50'36"E.). Calcite mapped near Quaternary intrusive rocks in the northwestern region of the AOI is of particular importance. Vikhter and others (1976) suggest that the aragonite prospects near the Early Quaternary intrusives are genetically similar to those found at the Khanneshin carbonatite volcano (also known as the Khān Nishīn Ghar volcano) and contain barium, strontium, and rare-earth elements. To determine if this region did form under conditions similar to those found at Khanneshin, additional geophysical and geochemical characterization is needed. Gypsum maps in a 0.3-km cluster of pixels near lat 29°38'42"N., long 64°54'51"E. The pattern in the HyMap data and brightness in the TM data suggests this is probably an evaporite deposit. The area is bounded by two faults and the valley floor is relatively flat, making it an ideal location for this type of deposit.

The Panawuk and Muzdan prospects in the southern region do occur within the calcites and are in close proximity to large areas of chlorite or epidote. The four aragonite prospects in the northwest are located near intrusive rocks and may be associated with them.

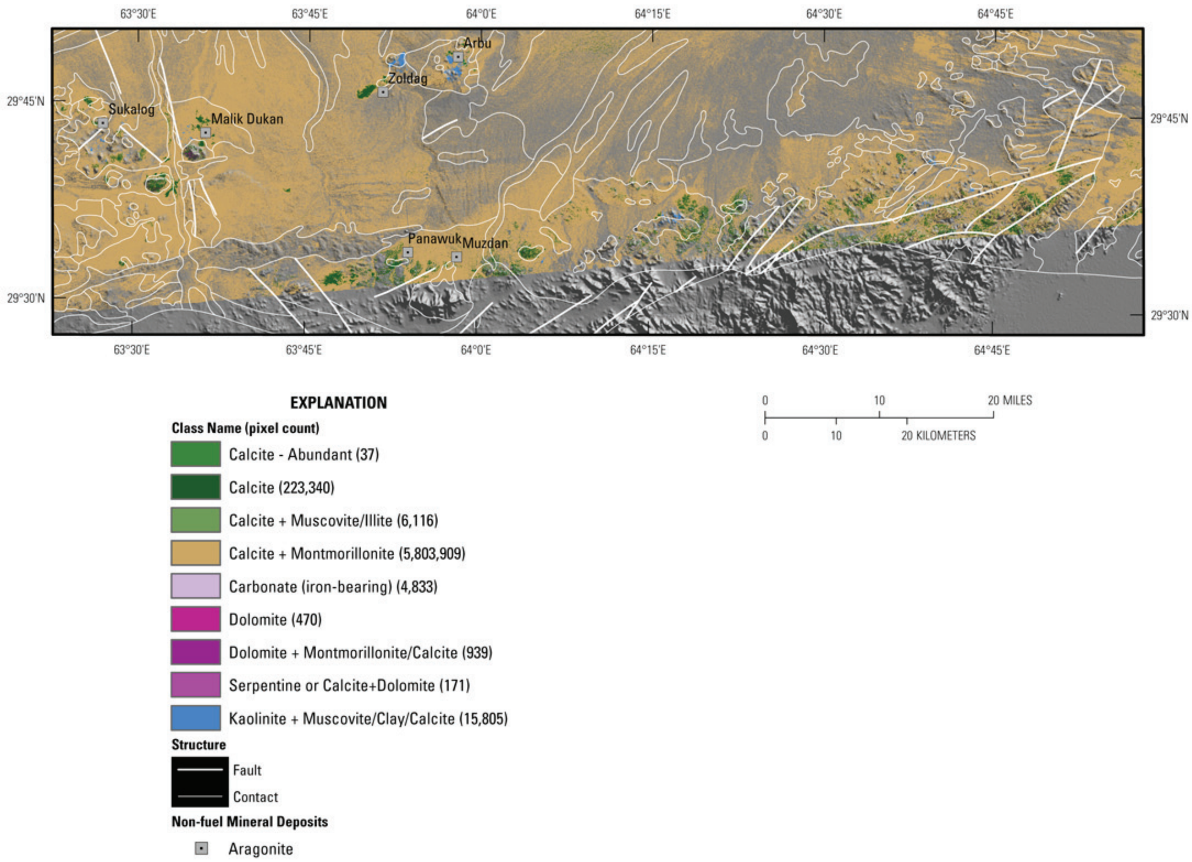

Figure 25B–8. Map of distribution of carbonate minerals derived from HyMap data in the South Helmand area of interest.

25B.4.2 Clays and Micas

The calcite + montmorillonite and calcite + muscovite/illite were removed from figure 25B–9 to improve clarity of the image because the calcite + clay/mica classes dominate the area. Illite with lesser amounts of muscovite are mapped over a significant portion of the AOI. Illite and muscovite appear to be associated with aeolian features throughout the area. Chlorite or epidote map within units of Cretaceous (undifferentiated) rocks in the southern Chaigai Hills area, and within spatially coherent groups in the western region. Montmorillonite maps near the gypsum area, within drainage systems in the central region, and within or near intrusive bodies in the western region of the South Helmand AOI. Montmorillonite concentrations occur within Early Quaternary rocks in the northwestern region. Montmorillonite is also present in alluvial fans in Early Pliocene rocks, and is mapped in Late Quaternary and Recent rocks in the western part of the AOI. Kaolinite + montmorillonite/clay/calcite are mapped in and around Early Quaternary intrusive rocks near lat 29°48'36"N., long 63°57'22"E. Many distinct areas of kaolinite group minerals occur in the South Helmand AOI. Kaolinite near lat 29°48'36"N., long 63°57'22"E., occurs in a region where several Early Quaternary intrusive bodies are exposed within stratified formations. Smaller clusters of kaolinite are mapped in a similar area 40 km southwest of this concentration (lat 29°41'42"N., long 63°26'45"E.). In the southern Chaigai Hills, kaolinite is mapped throughout Cretaceous (undifferentiated) formations and Oligocene intrusive rocks in both large and small spatially consistent patterns. Larger concentrations are located near lat 29°33'32"N., long 64°05'41"E., lat 29°37’02"N., long 64°17'18"E., lat 29°41'34"N., long 64°39'32"E., and lat 29°39'24"N., long 64°43'09"E. These concentrations have coherent groupings of kaolinite or kaolinite + muscovite/clay/calcite surrounded by muscovite or illite. Given the location, these areas may be associated with argillic hydrothermal alteration. Smaller groupings and single pixel detections occur near these four locations, and should also be looked at in more detail in future studies.

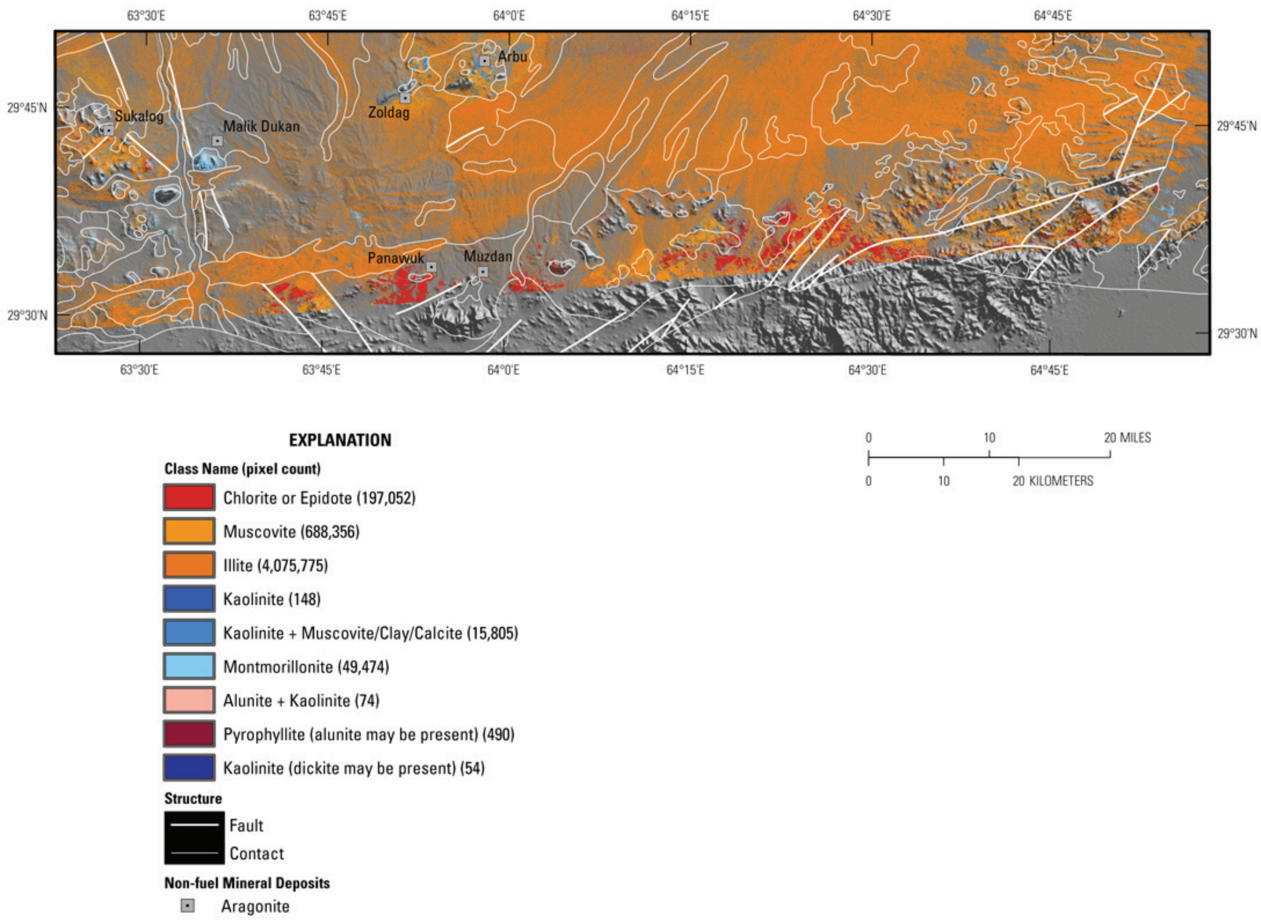

Figure 25B–9. Map of distribution of clay and mica minerals derived from HyMap data in the South Helmand area of interest.

25B.4.3 Iron Oxides and Hydroxides

The South Helmand AOI contains large areas of Fe-hydroxide, goethite and hematite (fig. 25B–10). Fe-hydroxide minerals generally occur in contiguous areas with Late Quaternary and Recent age rock across the AOI. Hematite is mapped in large concentrations near several intrusive complexes in the northwestern region of the AOI, and may be associated with weathering of these units. Hematite also forms a large arc-like structure near lat 29°38'36"N., long 64°41'04"E. Smaller coherent patterns of hematite occur throughout the Chaigai Hills and warrant additional analysis.

Goethite is mapped in large areas in the western region of the AOI in alluvial fans, as well as other geologic units. An outcrop near lat 29°39'23"N., long 64°43'03"E., that appears bright white in the TM data most closely matches the spectra of goethite, in the center with a ring of Fe3+ Type 1 and Fe-hydroxide; this area is shown in greater detail in King, Johnson, and others (2011).

Occurrences of jarosite are present throughout the Chaigai Hills area, and are most abundant along the southern boundary of the HyMap dataset. A series of three clusters of Jarosite occur near lat 29°36'44"N., long 64°39'44"E. Jarosite is also present in spatially consistent patterns associated with muscovite near lat 29°41'57"N., long 63°27'04"E., in the northwestern region of the AOI, and in a small but contiguous pattern near lat 29°37'57"N., long 64°57'11"E., in the southeast corner of the AOI. Jarosite minerals are often associated with advanced argillic rocks that have been hydrothermally altered. Smaller clusters or single-pixel occurrences of jarosite that map throughout the Chaigai Hills area should be investigated in greater detail. Jarosite is associated with the pyrophyllite class in the carbonates, phyllosilicates, sulfates, altered minerals, and other materials map near lat 29°36'52"N., long 64°32'55"E., in the southeastern region. In the south-central region near lat 29°37’02"N., long 64°17’18"E., jarosite is associated with kaolinite.

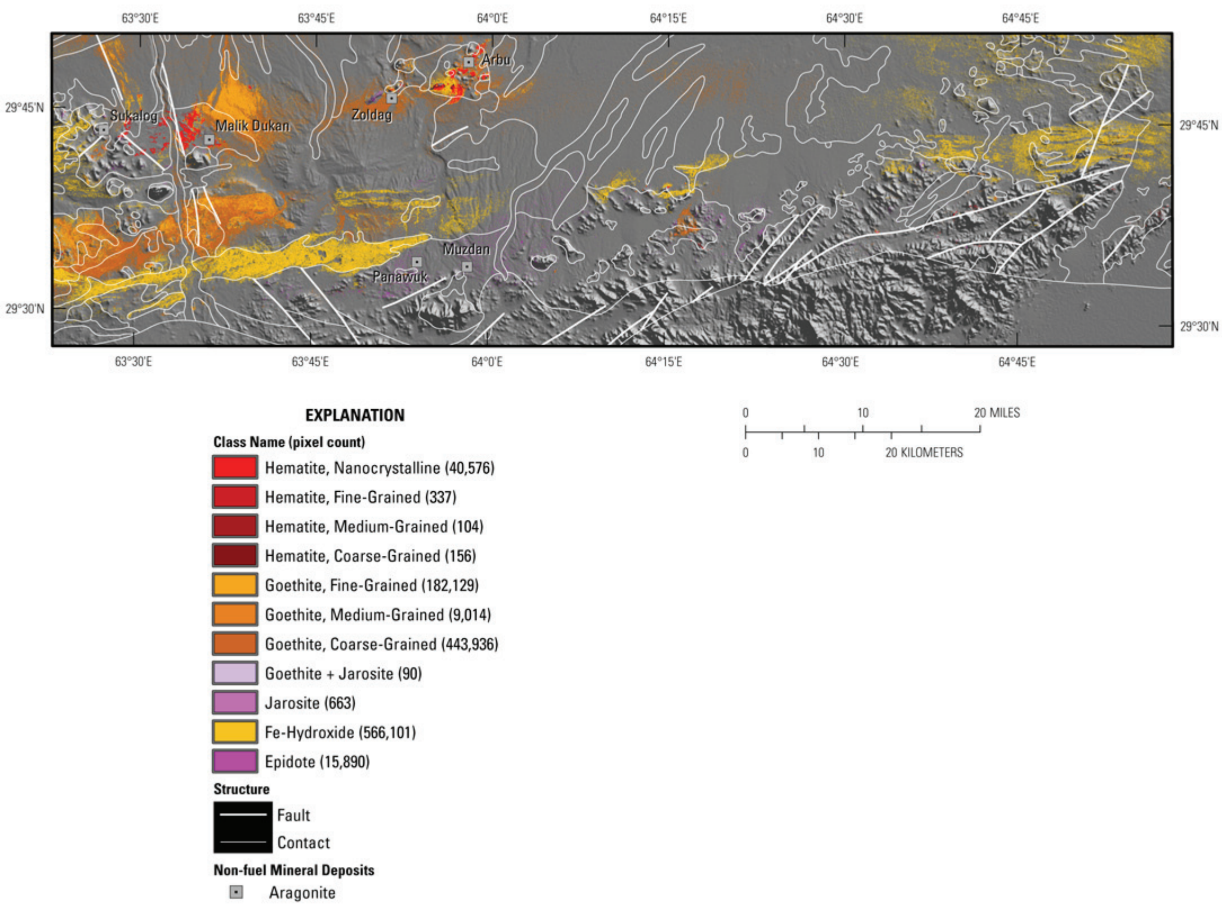

Figure 25B–10. Map of distribution of iron oxide and hydroxide derived from HyMap data in the South Helmand area of interest.

Epidote is dispersed throughout the AOI and does not occur in tight spatial groupings. A triangular area of jarosite, hematite, goethite, Fe-hydroxide and Fe3+ Type 1 occurs near lat 29°37'04"N., long 64°16'53"E. The classes detected here are unique for this area and should be investigated further. The area is shown in greater detail in King, Johnson, and others (2011).

25B.4.4 Common Alteration Minerals

Most of the minerals in this group are commonly present in hydrothermally altered rocks associated with epithermal mineral deposits (fig. 25B–11). Consequently, the locations of distinct clusters are of great interest in terms of potential mineral deposits. The South Helmand AOI contains significant clusters of hydrothermally altered rocks and should be examined in greater detail in order to assess the economic potential of the Chaigai Hills porphyry copper-gold area. The combination of chlorite or epidote, kaolinite, alunite, pyrophyllite and jarosite all indicate that this area contains argillic-advanced argillic hydrothermal alteration. Three significant, contiguous areas of pyrophyllite (possibly containing alunite) occur in the Chaigai Hills. The first area is located near lat 29°36'52"N., long 64°32'55"E. This oval-shaped pyrophyllite occurrence is 0.5 km wide and is bordered by pixels of alunite or alunite + kaolinite. The second area is located near lat 29°36'42"N., long 64°24'33"E. This cluster of pixels is approximately 0.25 km wide and 0.45 km long and is bordered by pixels of kaolinite + muscovite/clay/calcite. Another linear concentration of pyrophyllite occurs 1.35 km to the west of this cluster (lat 29°36'41"N., long 64°25'23"E.), and forms a narrow band 0.75 km long. This concentration also has kaolinite + muscovite/clay/calcite and alunite + kaolinite present. Very small groupings and individual pixels of pyrophyllite and (or) alunite are mapped throughout this area. Two coherent groupings of alunite, alunite + kaolinite and kaolinite (with a few pixels of pyrophyllite) occur at lat 29°33'22"N., long 64°12'18"E., and lat 29°33'14"N., long 64°10'17"E.; both detections are both approximately 0.5 km wide. The combination of kaolinite, alunite and pyrophyllite in these oval shaped patterns makes these occurrences a prime source for hydrothermally altered advanced argillic rocks, and is consistent with porphyry copper-gold mineralization. Many of these areas are shown in greater detail in King, Johnson, and others (2011).

25B.4.5 Common Secondary Minerals

The only mineral class highlighted in figure 25B–12 is the chlorite or epidote class along the southern edge of the HyMap data. This class is mapped in the Chaigai Hills and tends to be detected in areas of exposed bedrock. The epidote and serpentines shown do not occur in a spatially consistent pattern.

25B.5 Summary

The HyMap data for the South Helmand area indicate that several locations, based on the presence of specific minerals or groups of minerals, need additional field sampling, and geophysical and geochemical characterization. The HyMap data cover most of the AOI in this region, but the southern edge of the dataset prevents us from having complete coverage.

The dominant classes of materials are associated with aeolian sediments and bedrock in the map of iron-bearing minerals and the map of carbonates, phyllosilicates, sulfates, altered minerals, and other materials. Illite, Fe^{3+} Type 1 and Fe-hydroxide are mapped in spatial patterns consistent with aeolian sediments that can be seen in the TM data. Calcite + montmorillonite and Fe^{2+} Fe^{3+} Type 2 are detected in areas of exposed bedrock that have been blown free of aeolian sands.

Calcite that maps near Quaternary intrusive rocks in the northwestern region of the AOI are of particular importance. Vikhter and others (1976) suggest that the aragonite prospects near the Early Quaternary intrusive bodies are genetically similar to those found at the Khanneshin carbonatite volcano (Khān Nishīn Ghar volcano) and contain barium, strontium, and rare-earth elements. To determine if this region did form under conditions similar to those found at Khanneshin, additional geophysical and geochemical characterization is needed.

Kaolinite was mapped in or near Early Quaternary intrusive rocks in the northwestern region of the AOI. In the Chaigai Hills, kaolinite was detected in small areas associated with muscovite, alunite and pyrophyllite. These areas should be examined in greater detail, because they could be associated with argillic alteration.

Chlorite or epidote is mapped in large contiguous areas along the southern limit of the HyMap data. These areas occur at the higher elevations in the region that appear to be free of aeolian sediments.

Spectra matching minerals commonly associated with hydrothermal alteration mineral assemblages were mapped extensively in the southern Chaigai Hills area. Kaolinite, alunite, pyrophyllite and jarosite form large coherent groupings in several areas. Pyrophyllite was mapped in three areas with two of them forming round masses that were bordered by pixels matching the spectra of alunite, alunite + kaolinite or kaolinite. The largest of the areas is located near lat 29°36'52"N., long 64°32'55"E. Several areas rich in alunite were found and were also bordered by pixels of kaolinite, with a few scattered pixels of pyrophyllite also present. The largest two areas are located near lat 29°33'22"N., long 64°12'18"E., and lat 29°33'14"N., long 64°10'17"E.

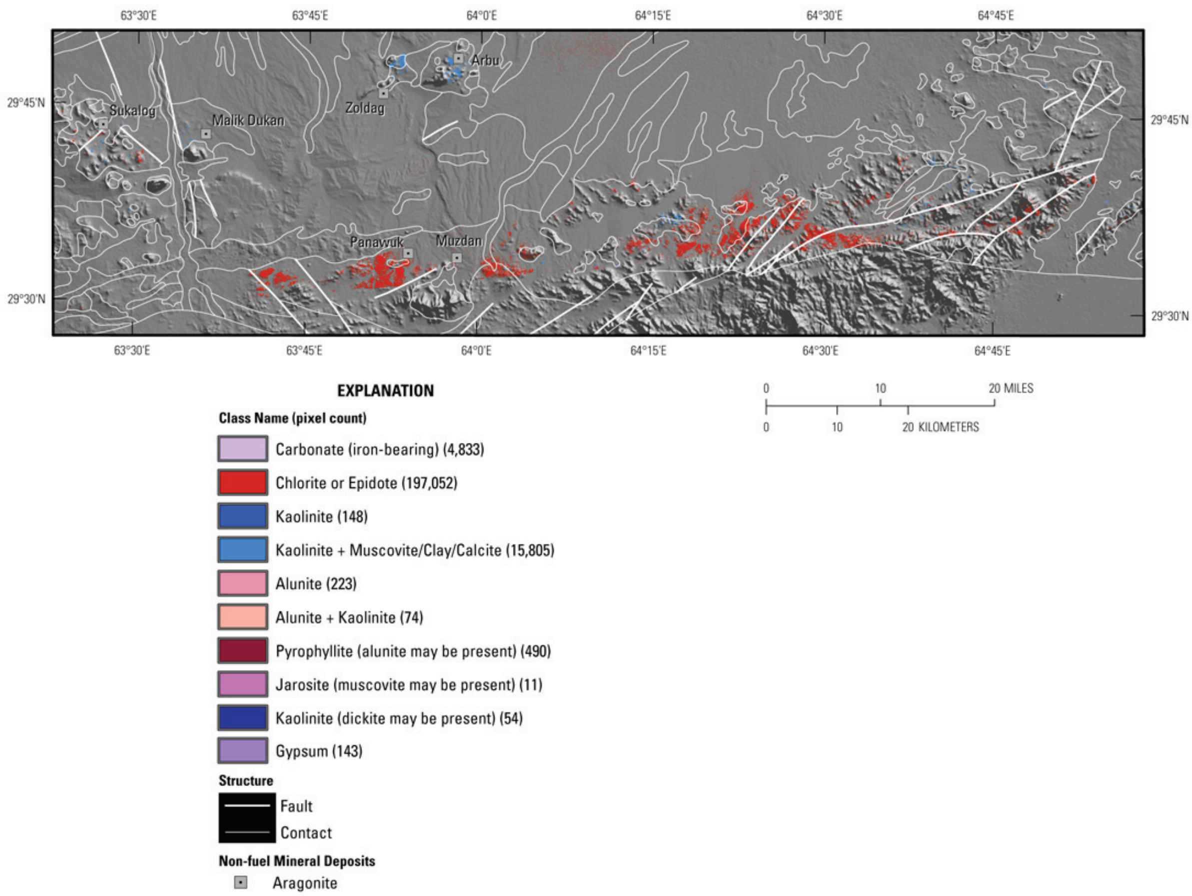

Figure 25B–11. Map of distribution of common alteration minerals derived from HyMap data in the South Helmand area of interest.

Jarosite is associated with pyrophyllite, kaolinite, and strong detections of muscovite in the carbonates, phyllosilicates, sulfates, altered minerals, and other materials map (figure 25B–6). Most of the jarosite detections were found in the southern Chaigai Hills, with the exception of a few concentrations near Early Quaternary intrusive rocks in the northwestern region of the AOI.

The HyMap data for the South Helmand AOI clearly show areas of mapped minerals that are consistent with the materials commonly associated with the known mineral occurrences in the area (table 25B–1). The HyMap data have identified several areas of hydrothermal alteration that are consistent with minerals that are found in porphyry copper-gold systems, and these areas warrant additional investigation including field work, and geophysical and geochemical studies.

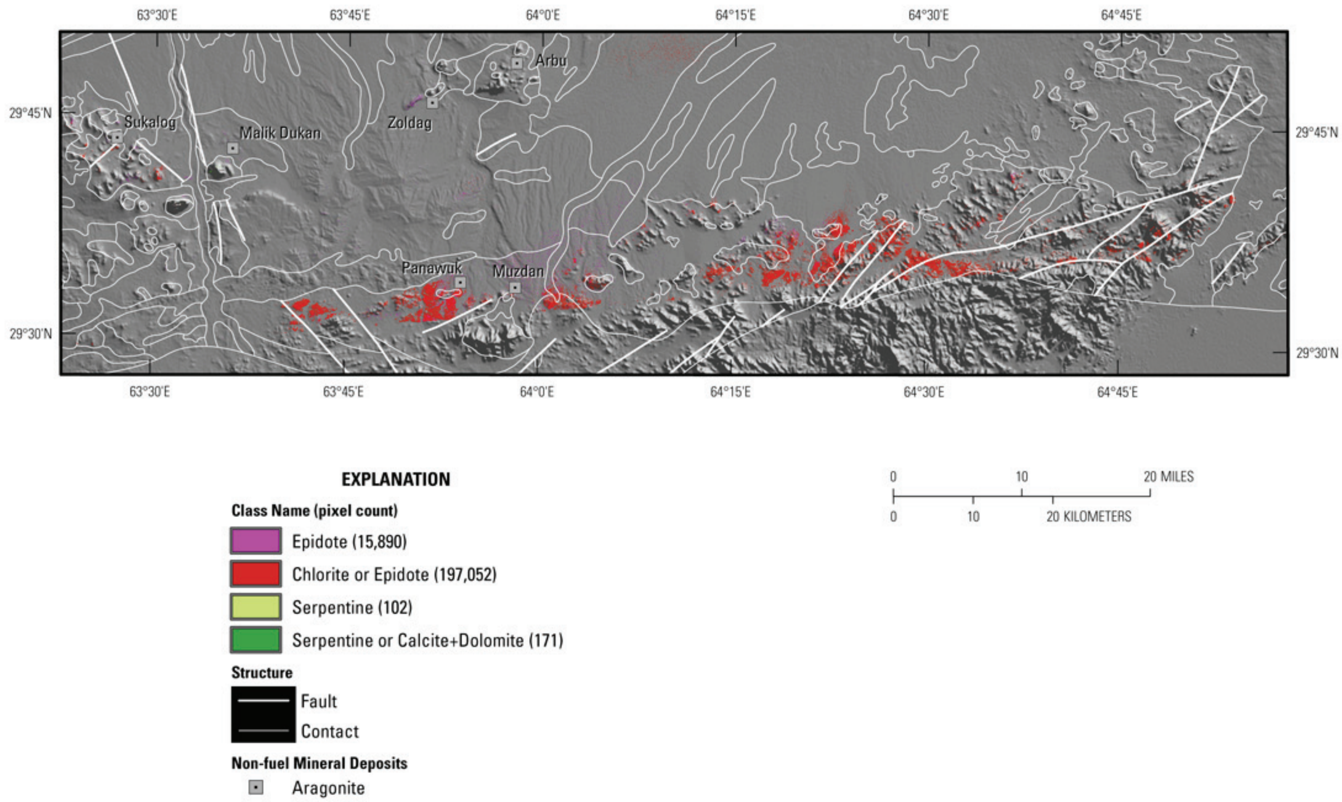

Figure 25B–12. Map of distribution of common secondary minerals derived from HyMap data in the South Helmand area of interest.

25B.6 References Cited

Abdullah, Sh., and Chmyriov, V.M., 1977, Geological map of Afghanistan: Kabul, Afghanistan, Ministry of Mining and Industry of Democratic Republic of Afghanistan, scale 1:500,000.

Abdullah, Sh., Chmyriov, V.M., Stazhilo-Alekseev, K.F., Dronov, V.I., Gannan, P.J., Rossovskiy, L.N., Kafarskiy, A.Kh., and Malyarov, E.P., 1977, Mineral resources of Afghanistan (2d ed.): Kabul, Afghanistan, Republic of Afghanistan Geological and Mineral Survey, 419 p.

Ahmad, M.U., 1992, Porphyry copper in Pakistan: Geological Survey of Pakistan, no. 9, 21 p.

Ahmad, M.U., Siddiqui, R.H., and Chaudhary, M.A., 1986, Geological and geochemical exploration and preliminary evaluation of Dasht-e-Kain porphyry copper-molybdenum prospect, Chagai district, Baluchistan, Pakistan: Geological Survey of Pakistan, Mineral Resources Records, v. 72, 44 p.

Breitzman, L.L., Birnie, R.W., and Johnson, G.D., 1983, Fission-track ages of the Chagai intrusives, Baluchistan, Pakistan: Geological Society of America Bulletin, v. 94, p. 253–258.

Cocks, T., Jenssen, R., Stewart, A., Wilson, I., and Shields, T., 1998, The HyMap airborne hyperspectral sensor—The system, calibration and performance, *in* Schaepman, M., Schlapfer, D., and Itten, K.I., eds., Proceedings of the 1st EARSeL Workshop on Imaging Spectroscopy, 6–8 October 1998, Zurich: Paris, European Association of Remote Sensing Laboratories, p. 37–43.

Davis, P.A., 2007, Landsat ETM+ false-color image mosaics of Afghanistan: U.S. Geological Survey Open-File Report 2007–1029, 22 p. (Also available at *http://pubs.usgs.gov/of/2007/1029/*.)

Doebrich, J.L., and Wahl, R.R., comps., *with contributions by* Doebrich, J.L., Wahl, R.R., Ludington, S.D., Chirico, P.G., Wandrey, C.J., Bohannon, R.G., Orris, G.J., Bliss, J.D., and ____, 2006, Geologic and mineral resource map of Afghanistan: U.S. Geological Survey Open File Report 2006–1038, scale 1:850,000, available at *http://pubs.usgs.gov/of/2006/1038/*.

Hoefen, T.M., Kokaly, R.F., and King, T.V.V., 2010, Calibration of HyMap data covering the country of Afghanistan, *in* Proceedings of the 15th Australasian Remote Sensing and Photogrammetry Conference, Alice Springs, Australia, September 12–17, 2010, p. 409, available at *http://dl.dropbox.com/u/81114/15ARSPC-Proceedings.zip/*.

Kazmi, A.H., and Qasim Jan, M., 1997, Geology and tectonics of Pakistan: Graphic Publishers, Karachi, 554 p.

King, T.V.V., Kokaly, R.F., Hoefen, T.M., and Knepper, D.H., 2010, Resource mapping in Afghanistan using HyMap data, *in* Proceedings of the 15th Australasian Remote Sensing and Photogrammetry Conference, Alice Springs, Australia, September 12–17, 2010, p. 500, available at *http://dl.dropbox.com/u/81114/15ARSPC-Proceedings.zip/*.

King, T.V.V., Johnson, M.R., Hoefen, T.M., Kokaly, R.F., and Livo, K.E., 2011, Mapping potential mineral resource anomalies using HyMap data, *in* King, T.V.V., Johnson, M.R., Hubbard, B.E., and Drenth, B.J., eds, Identification of mineral resources in Afghanistan—Detecting and mapping resource anomalies in prioritized areas using geophysical and remote sensing (ASTER and HyMap) data in Afghanistan: U.S. Geological Survey Open-File Report 2011–1229, available at *http://pubs.usgs.gov/of/2011/1229/*.

King, T.V.V., Kokaly, R.F., Hoefen, T.M., Dudek, K. and Livo, K.E., 2011, Surface materials map of Afghanistan—Iron-bearing minerals and other materials: U.S. Geological Survey Scientific Investigations Map 3152–B.

Kokaly, Ray, 2011, PRISM—Processing routines in IDL for spectroscopic measurements: U.S. Geological Survey Open-File Report 2011–1155, available at *http://pubs.usgs.gov/of/2011/1155/*.

Kokaly, R.F., King, T.V.V., Hoefen, T.M., Dudek, K. and Livo, K.E., 2011, Surface materials map of Afghanistan—Carbonates, phyllosilicates, sulfates, altered minerals, and other materials: U.S. Geological Survey Scientific Investigations Map 3152–A.

Kokaly, R.F., King, T.V.V., and Livo, K.E., 2008, Airborne hyperspectral survey of Afghanistan 2007—Flight line planning and HyMap data collection: U.S. Geological Survey Open-File Report 2008–1235, 14 p.

Leaman, P., and Staude, J.M., 2003, Metallogenic evolution of the western Tethys of Turkey and Iran: MMAJ Forum Presentation, 24 p., accessed January 10, 2011, at *www.mmaj.go.jp/mric_web/MMAJ_Forum*.

Mars, J.C., and Rowan, L.C., 2007, Mapping phyllic and argillic-altered rocks in southeastern Afghanistan using advanced spaceborne thermal emission and reflection radiometer (ASTER) data: U.S. Geological survey Open-File Report 2007-1006. (Also available at http://pubs.usgs.gov/of/2007/1006/.)

Perello, J., Razique, A., Schloderer, J. and Rehman, A., 2008, The Chagai Porphyry Copper Belt, Baluchistan Province, Pakistan: Economic Geology, v. 103, no. 8, p. 1583–1612

Peters, S.G., Ludington, S.D., Orris, G.J., Sutphin, D.M., Bliss, J.D., and Rytuba, J.J., eds., and the U.S. Geological Survey-Afghanistan Ministry of Mines Joint Mineral Resource Assessment Team, 2007, Preliminary non-fuel mineral resource assessment of Afghanistan: U.S. Geological Survey Open-File Report 2007–1214, 810 p., 1 CD–ROM. (Also available at *http://pubs.usgs.gov/of/2007/1214/*.)

Sillitoe, R.H., 1978, Metallogenic evolution of a collisional mountain belt in Pakistan: A preliminary analysis: Journal of the Geological Society of London, v. 135, p. 377–387.

Sillitoe, R.H., and Khan, S.N., 1977, Geology of Saindak porphyry copper deposit, Pakistan: Institution of Mining and Metallurgy Transaction Section B, v. 86, p. B27–B42.

Spector, A., Hood, P.J., Farah, A., and Ahmed, W., 1987, Applications of aeromagnetic data to mineral-resources exploration—Baluchistan, Pakistan, *in* Kane, M.F., O'Hara, N.W., Redford, M.S., Tanner, J., and Weber, C., eds., The Utility of Regional Gravity and Magnetic Anomaly Maps: Tulsa, Okla., Society of Exploration Geophysicists, p. 132-143.

Vikhter, B.Y., Yeremenko, G.K., and Chmyrev, V.M., 1976, A young volcanogenic carbonatite complex in Afghanistan: International Geology Review, v. 18, no. 11, p. 1305–1312.